Minimization of cross-talk between Spindle Assembly Checkpoint silencing and error correction

Babhrubahan Roy[1], Vikash Verma[1,+], Janice Sim[1], Adrienne Fontan[1], Ajit P. Joglekar[1,2]

1 – Cell & Developmental Biology, University of Michigan Medical School, Ann Arbor

2 – Biophysics, University of Michigan, Ann Arbor

+ - Current address: Biology department, University of Massachusetts, Amherst

Correspondence to: ajitj@umich.edu

Abstract

Accurate chromosome segregation during cell division requires that sister kinetochores attach to microtubules originating from opposite spindle poles. This is ensured by the Spindle Assembly Checkpoint (SAC), which detects unattached kinetochores, and an error correction mechanism that detects and destabilizes incorrect attachment of both sister kinetochores to the same spindle pole. Both these processes are regulated by Protein Phosphatase 1 (PP1). PP1 silences the SAC and stabilizes correct, bipolar kinetochore-microtubule attachments. We show that this dual role of PP1 can be problematic. Premature recruitment of PP1 to the kinetochore for SAC silencing interferes with efficient error correction, because PP1 can then inadvertently stabilize incorrect attachments. The yeast kinetochore mitigates this cross-talk by: (a) using independent sources of PP1 for attachment stabilization and SAC silencing, and (b) delaying PP1 recruitment for SAC silencing until correct attachments are established. Thus, error correction precedes SAC silencing, and ensures accurate chromosome segregation.

Introduction

The eukaryotic kinetochore performs three distinct functions to segregate chromosomes: spindle assembly checkpoint signaling, force generation, and error correction (Joglekar and Kukreja, 2017). The molecular mechanisms of these functions are quite distinct. Yet, their operation *in vivo* is intertwined, in part because these functions are regulated by the same kinases and phosphatases. In particular, Protein Phosphatase 1 (PP1) plays key roles in both SAC and error correction. PP1 silences the SAC by promoting the unbinding of SAC proteins from the kinetochore (London et al., 2012; Meadows et al., 2011; Nijenhuis et al., 2014; Rosenberg et al., 2011). It plays an indirect role in error correction by stabilizing end-on kinetochore-microtubule attachments (Liu et al., 2010; Posch et al., 2010; Suzuki et al., 2018). However, to ensure accurate chromosome segregation, these two PP1 functions must be separated from one another, and executed sequentially. This is because end-on kinetochore microtubule attachments disrupt SAC signaling, irrespective of whether these attachments are bipolar or syntelic (Etemad et al., 2015; Tauchman et al., 2015). If PP1 is recruited to the kinetochore as soon as end-on attachments form, then PP1 will not only silence the SAC, but it may also inadvertently dephosphorylate microtubule-binding kinetochore proteins, and stabilize erroneous kinetochore-microtubule attachments. If this potential cross-talk in the two PP1 functions is not avoided, the result will be elevated chromosome missegregation (Fig. 1A). Therefore, the temporal regulation of PP1 recruitment and activity in the kinetochore is likely to be crucial to ensure that error correction and SAC silencing do not interfere with one another.

The well-known factor for PP1 recruitment to the kinetochore for SAC silencing is the conserved kinetochore protein Spc105/KNL1. The N-terminus of Spc105 harbors two PP1-interacting motifs: the primary ‘RVSF’ motif and the secondary ‘SILK’ motif (Hendrickx et al., 2009; Liu et al., 2010; London et al., 2012; Nijenhuis et al., 2014; Rosenberg et al., 2011). The Serine residues in both these motifs are phosphorylated by Aurora B, which inhibits their ability to bind PP1 (Liu et al., 2010). However, this inhibition of PP1 recruitment by Aurora B is mainly thought enhance the recruitment of SAC proteins, and contribute to robust SAC signaling (Nijenhuis et al., 2014). The possibility that this inhibition is crucial for efficient error correction has not been considered. To investigate the role of regulated PP1 recruitment in coordinating SAC silencing and error correction, we re-examined the cell biological function of the regulation of PP1 interaction with Spc105 in budding yeast.

Results and Discussion

A conserved basic patch near the N-terminus of Spc105 contributes to Glc7 recruitment

To understand the role of phosphoregulation of the PP1-Spc105 interaction in budding yeast, we first examined how the phosphorylation of Spc105 affects its interaction with PP1, known as Glc7 in budding yeast. The RVSF motif of Spc105 is phosphorylated by Ipl1 (Aurora B), but abrogation of this phosphoregulation does not appear to have adverse effects on either chromosome segregation or SAC signaling (Rosenberg et al., 2011). Spc105 contains a variant of the 'SILK' motif, an auxiliary Glc7 binding site, wherein the non-phosphorylatable Glycine occupies the position of the Serine residue (Fig. 1B). Thus, the phosphoregulation of the known PP1 recruitment site is unlikely to play a detectable role in SAC signaling in budding yeast. Therefore, we hypothesized that the conserved patch of four basic residues: 'RRRK' (a.a. 101-104, Fig. 1B), in the N-terminus of Spc105 may function as an additional, phosphoregulatable Glc7 binding site. Our conjecture was based on three observations. First, mutation of a similar basic patch in KNL1 in *C. elegans* led to phenotypes consistent with impaired SAC silencing: retention of the Bub3, an SAC signaling protein that is removed by PP1-mediated dephosphorylation of KNL1, in metaphase kinetochores, and delayed anaphase onset (Espeut et al., 2012). Second, the basic patch may contribute to Glc7 recruitment by interacting electrostatically with the negatively charged surface of Glc7 (Hurley et al., 2007). Finally, basic patch activity can be disrupted by phosphorylation of the Serine and Threonine residues immediately downstream. To test our hypothesis, we created a basic patch mutant (BPM) $Spc105^{BPM}$, wherein the basic residues in two distinct basic patches: an anterior one spanning residues 101-104 and a posterior one spanning residues 340-343, are replaced with non-polar alanine residues. Mutation of either one or both basic patches in Spc105 showed no adverse effects on cell growth or viability (Fig. S1A). It will be shown later that only the anterior basic patch is involved in the phenotypes and processes discussed here.

Study of the basic patch in *C. elegans* suggested that the basic patch in KNL1 binds to microtubules (Espeut et al., 2012). Therefore, we first tested whether the same is true for Spc105. Using single molecule microscopy, we could not detect interaction of recombinant Spc105 phosphodomains with Taxol-stabilized porcine microtubules at the physiological salt concentration (data not shown). However, when wild-type Spc105 phosphodomain molecules were concentrated on microspheres, the microspheres readily bound to microtubules. This binding was abrogated when the basic patches were mutated (Fig. 1C). These results suggest that the basic patch may facilitate a weak interaction of the Spc105 phosphodomain with the

microtubule. Therefore, we analyzed whether Spc105^{BPM} perturbs the kinetics of kinetochore biorientation and force generation. We released yeast cells expressing either Spc105 or Spc105^{BPM} from a G1 arrest and periodically analyzed kinetochore biorientation in the cell population using a previously described method (Marco et al., 2013). We found that cells expressing Spc105^{BPM} bioriented their kinetochores faster as compared to cells expressing wild-type Spc105 (compare the V-plots in Fig. 1D displaying kinetochore distribution over > 50 spindles imaged at the indicated times after release from the G1 arrest). The average distance between the centroids of sister kinetochore clusters was also higher in cells expressing Spc105^{BPM} even though the spindle length remained unchanged (scatterplots in Fig. 1D). The increased separation between sister kinetochores is indicative of enhanced force generation. Thus, rather than reducing kinetochore force generation, Spc105^{BPM} enhances both kinetochore biorientation and force generation.

We next assessed the effect of Spc105^{BPM} on SAC signaling by quantifying Bub3 recruitment in bioriented kinetochores in metaphase. Bub3 binds to phosphorylated MELT motifs in Spc105 as a part of the Bub3-Bub1 complex (Aravamudhan et al., 2015; Hiruma et al., 2015; Ji et al., 2015; London et al., 2012; Primorac et al., 2013). Glc7 dephosphorylates the MELT motifs to suppress Bub3 recruitment (London et al., 2012). Normally, only a minority of metaphase-arrested yeast cells show detectable Bub3 recruitment (Fig. 1E). However, bioriented kinetochores in most yeast cells expressing either Spc105^{BPM} or Spc105^{ABPM} (wherein only the anterior basic patch is mutated) recruited, or retained, significantly higher amounts of Bub3-Bub1 even in metaphase (Fig. 1E). Interestingly, most cells expressing Spc105^{BPM} failed to recruit detectable levels of Mad1 (Fig. 1E, micrographs and quantification shown in Fig. S1B). These data reveal that Spc105^{BPM} abnormally promotes either the recruitment or retention of Bub3-Bub1 at kinetochores even in metaphase.

The abnormal Bub3-Bub1 recruitment or retention can be explained by two different mechanisms. First, Spc105^{BPM} may promote the retention of Bub3-Bub1 by simply reducing Glc7 recruitment or activity and thus suppressing the dephosphorylation of MELT motifs. Alternatively, reduced microtubule-binding ability of Spc105^{BPM} may promote Bub3-Bub1 recruitment by enabling the MELT motifs to interact with Mps1 bound to the CH-domains of the Ndc80 complex (Aravamudhan et al., 2015). To understand which of the two mechanisms is responsible for the observations described above, we tested whether the phenotype is suppressed by the re-introduction the basic patch in Spc105^{BPM}. We reasoned that if the microtubule-binding activity of the basic patch is responsible for the abnormal Bub3-Bub1

recruitment, then re-introduction of just this activity should suppress it (electrostatic interaction between the basic patch and the negatively charged E-hooks of tubulin should occur independently of its position). We created two variants of Spc105^{BPM} by fusing a fragment of Spc105 spanning either just the basic patch and its surrounding residues, or the basic patch along with the RVSF motif to the N-terminus of Spc105^{BPM} (shown in Fig. 1F). We found that the reintroduction of the basic patch alone did not suppress the abnormal Bub3 recruitment, but the reintroduction of the RVSF motif and the basic patch together did (Fig. 1F, graph). These data strongly suggest that the basic patch and the RVSF motif act together to recruit Glc7 activity in the yeast kinetochore, and that the microtubule-binding activity alone is not sufficient to suppress Bub3 recruitment/retention in metaphase kinetochores.

To directly test whether the basic patch contributes to Glc7 recruitment by Spc105, we next concentrated four versions of recombinant Spc105 phosphodomains: wild-type, Spc105^{RASA} (wherein the RVSF motif is non-functional), Spc105^{BPM}, Spc105$^{\Delta 80\text{-}128}$ (wherein residues spanning the basic patch are deleted) on GFP-trap beads, and quantified the amount of Myc-tagged Glc7 from yeast lysates that co-precipitated with these beads (Fig. S1C). Mutation of the RVSF motif reduced Glc7 co-precipitation to background levels indicating that the basic patch does not recruit Glc7 on its own. We could not reliably detect a difference in the amount of Glc7 co-precipitating with the wild-type and Spc105^{BPM} phosphodomains in this assay. Nonetheless, Glc7 amount was reduced in the case of Spc105$^{\Delta 80\text{-}128}$.Therefore, we conclude that the basic patch and its surrounding residues contribute to RVSF motif-mediated recruitment of Glc7. Any potential microtubule-binding activity of the basic patch is unlikely to be important for the phenotypes discussed here.

Spc105^{BPM} does not enhance SAC signaling

Involvement of the basic patch and its surrounding residues in Glc7 recruitment prompted us to study whether Spc105^{BPM} affects SAC signaling and silencing. We treated cells expressing either wild-type Spc105 or Spc105^{BPM} with the microtubule poison nocodazole to depolymerize the spindle and create unattached kinetochores. In both cases, unattached kinetochores recruited similar amounts of Bub3 indicating that SAC signaling activity is unaffected by the mutation (Fig. 2A). This observation is consistent with our prior finding that Glc7 inhibition has no effect on Bub3 recruitment in unattached kinetochores in budding yeast (Aravamudhan et al., 2016). We next used flow cytometry to quantify changes in the DNA content of cells treated with

nocodazole over time. Spc105^{BPM} had no detectable effect on the ploidy, indicating that the strength of SAC signaling was not detectably unaffected by the mutation (Fig. 2B). Finally, we tested whether Spc105^{BPM} delays the metaphase to anaphase transition by monitoring its timing in a synchronized cell population. Consistent with results from *C. elegans*, the metaphase-to-anaphase transition was also slightly delayed in cells expressing Spc105^{BPM} (Fig. 2C). Together, these results show that Spc105^{BPM} has minimal impact on SAC signaling, but causes a minor impairment of SAC silencing, consistent with the involvement of the basic patch in Glc7 recruitment to the kinetochore.

Spc105^{BPM} significantly improves error correction in an Sgo1-independent manner

The enhancement in the kinetics of kinetochore biorientation in cells expressing Spc105^{BPM} (Fig. 1D) is counter-intuitive, because reduced Glc7 recruitment via Spc105 should reduce the dephosphorylation of microtubule-binding kinetochore proteins and thus slow down the stabilization of kinetochore-microtubule attachments. Therefore, we next investigated the mechanism behind this surprising observation. An obvious candidate mechanism involves the upregulation of centromeric Sgo1 recruitment due to the abnormal Bub3-Bub1 retention at kinetochores (Fig. S2A). Higher Sgo1 recruitment will in turn enhance sister centromere cohesion and Aurora B activity thus resulting in better biorientation and error correction (Kawashima et al., 2010a; Kawashima et al., 2010b; Peplowska et al., 2014; Salic et al., 2004). To test this notion, we used the benomyl sensitivity assay to detect genetic interactions between factors involved in the Sgo1-mediated error correction pathway and Spc105^{BPM} (see Fig. 3A for a schematic of the error correction pathway). In this assay, yeast cells are grown on media containing low doses of the drug benomyl. In the presence of benomyl, microtubule dynamicity decreases significantly, and as a result, the spindle becomes short, oscillatory movements of bioriented kinetochores dampen, and centromeric tension is significantly reduced (Pearson et al., 2003). To proliferate under these conditions, yeast cells must use the SAC and error correction mechanisms together to accurately segregate their chromosomes. Therefore, mutant strains that are defective in either SAC signaling (e.g. *mad2Δ*) or error correction (e.g. *sgo1Δ*) grow poorly or are inviable on benomyl-containing media, even though they are viable on normal media (Fig. 3B).

The single mutants *bub1$^{\Delta kinase}$* (which expresses Bub1 lacking its kinase domain) or *sgo1Δ* have a functional SAC (Fig. S2B), but impaired error correction. They grow on normal media, but they

cannot grow on benomyl-containing media (Fig. 3Bi and ii). Strikingly, the double mutants *spc105*^{BPM} *bub1*$^{\Delta kinase}$ and *spc105*^{BPM} *sgo1Δ* grew on benomyl-containing media (Figure 3Bi and ii). The positive genetic interaction shows that Spc105^{BPM} enhances kinetochore biorientation independently of Sgo1. Using this functional readout, we confirmed that mutation of only the anterior basic patch (Spc105^{ABPM}), but not the posteriorly located basic patch (Spc105^{PBPM}), suppresses the benomyl-lethality of *sgo1Δ* cells (Fig. S2C). Similarly, *spc105*$^{\Delta 80\text{-}128}$, the Spc105 mutant wherein the basic patch and the residues surrounding it are deleted, also strongly suppressed the benomyl-sensitivity of *sgo1Δ* cells (Fig. 3Bii). Furthermore, only Spc105^{EBP1}, but not Spc105^{EBP2}, suppressed the benomyl-sensitivity of *sgo1Δ* (Fig. S2D). These results further support our conclusion that the basic patch and its surrounding residues contribute to Glc7 recruitment. They also show that reduced Glc7 activity in the kinetochore leads to improved error correction.

To further understand how Spc105^{BPM} improves error correction, we studied genetic interactions between *spc105*^{BPM} and known factors in sister kinetochore biorientation and error correction (see pathway in the cartoon in Figure 3A). *spc105*^{BPM} suppressed the benomyl-lethality of the deletion of the gene *RTS1* (Fig. 3Biii), which encodes a regulatory subunit of the Protein Phosphatase 2A involved in sister chromatid cohesion (Peplowska et al., 2014; Xu et al., 2009). *spc105*^{BPM} rescued the temperature sensitivity of a strain expressing *ipl1-2* (Ipl1-H352Y) that has a weaker kinase activity (Figure 3B-iv). Finally, we tested genetic interactions between *spc105*^{BPM} and mutations in the kinetochore proteins Ndc80 and Dam1 that render known Ipl1 phosphorylation sites within the respective protein non-phosphorylatable (mutated phosphosites indicated at the bottom) (Cheeseman et al., 2002; Lampson et al., 2004; Pinsky et al., 2006b; Tanaka et al., 2002). These mutations are expected to create hyper-stable kinetochore-microtubule attachments, and thus interfere with error correction. *spc105*^{BPM} suppressed the benomyl sensitivity in both cases, and even in strain carrying both mutations (Figure 3B-v and vi).

These results demonstrate that *spc105*^{BPM} enhances error correction in a Sgo1-independent manner. Our biochemical data indicate that the improvement in error correction is mainly due to reduced Glc7 recruitment by Spc105. However, these findings don't simply reinforce the notion that Ipl1 and Glc7 activities must be precisely balanced to ensure accurate chromosome segregation (Pinsky et al., 2006a; Tatchell et al., 2011). In this regard, the suppression of the benomyl-sensitivity of the *rts1Δ* mutant by *spc105*^{BPM} is especially noteworthy, because *rts1Δ* does not affect centromeric enrichment of either Sgo1 or Ipl1 (Peplowska et al., 2014).

Therefore, Ipl1 activity at the centromere should be unaffected in this mutant. Yet, *spc105*^{BPM} counteracts the benomyl-sensitivity of this mutation. Thus, *spc105*^{BPM} acts as a gain of function mutation by reducing Glc7 recruitment to the kinetochore via Spc105.

Glc7 recruited via the RVSF motif in Spc105 is not required for error correction

A key implication of the above findings is that the benomyl sensitivity of yeast cells is predominantly due to their inability to ensure bipolar attachments rather than SAC signaling. We directly confirmed this implication by demonstrating that *spc105*^{BPM} restored the viability of *mad2Δ* cells on media containing benomyl (Fig. 4A and S3A). We further exploited this observation to test whether kinetochore biorientation is adversely affected due to the Glc7 recruited specifically via Spc105. We analyzed the process of kinetochore biorientation in a strain expressing Spc105^{RASA} but lacking Mad2, because the SAC must be inactivated to obtain viable yeast cells expressing Spc105^{RASA} (Fig. S3B) (Rosenberg et al., 2011). As before, we first quantified the distribution of fluorescently labeled kinetochores as cells progressed from G1 to metaphase (Fig. 4B). Similar to *spc105*^{BPM}, *spc105*^{RASA} significantly improved the kinetics of kinetochore biorientation and kinetochore force generation, but minimally affected spindle length (Figure 4B).

It remained possible that the reduced recruitment of Glc7 by Spc105^{BPM} leads to stronger SAC signaling only in the presence of small numbers of unattached kinetochores. Importantly, cells grown on benomyl-containing media are likely to contain a few unattached kinetochores, whereas nocodazole-treated cells typically contain 8-10 unattached kinetochores (Aravamudhan et al., 2016). If this were the case, then the improved error correction could be the result of the extra time in mitosis afforded to the unattached kinetochores by the stronger checkpoint. To directly test this notion, we used the benomyl sensitivity assay as a functional test of the efficacy of the error correction process in *spc105*^{RASA} *mad2Δ* cells. As in the case of *spc105*^{BPM}, *spc105*^{RASA} *mad2Δ* grew robustly on benomyl-containing media, even though *mad2Δ* grew poorly under the same condition (Fig. 4C). *spc105*^{RASA} also mildly suppressed the benomyl lethality due to *bub3Δ* (Fig. S3B). Perhaps most strikingly, the triple mutant *spc105*^{RASA} *mad2Δ sgo1Δ* was able to grow on benomyl-containing media showing that the elimination of Glc7 recruitment via Spc105 significantly improves kinetochore biorientation and error correction (Fig. 4D).

These data establish two key points. First, Glc7 recruited by the RVSF motif of Spc105 is not required for error correction as inferred from the benomyl resistance of cells expressing Spc105^{RASA}. The stabilization of bipolar attachments is achieved by an Spc105-independent Glc7 activity. Second, our data imply that Glc7 recruited by the RVSF motif interferes with error correction, presumably by inadvertently stabilizing erroneous end-on attachments, , because cells expressing Spc105^{RASA} or Spc105^{BPM} achieve faster kinetochore biorientation. This reason may explain the nature of *spc105^{BPM}* as a gain of function mutation.

Spc105^{BPM} improves the accuracy of chromosome segregation

To test whether reduced Glc7 recruitment via Spc105 improves the accuracy of chromosome segregation, we observed chromosome segregation by fluorescently marking the centromere on chromosome IV using Tet-operator (TetO) repeats inserted proximal to the centromere. We first destroyed the spindle by treating cells with nocodazole, and then monitored spindle formation and the kinetics of chromosome IV biorientation (Verzijlbergen et al., 2014). Consistent with our expectation, TetO spots marking centromere IV separated from one another faster in cells expressing Spc105^{BPM} as compared to wild-type cells (Fig. 4E, right). Importantly, the frequency of chromosome IV missegregation was significantly reduced in cells expressing Spc105^{BPM}. Thus, reduced Glc7 recruitment by Spc105 leads to improved kinetochore biorientation and reduced chromosome segregation errors in the *sgo1Δ* background.

Phosphoregulation of Spc105 can mitigate the cross-talk between SAC silencing and error correction

Our results imply that the recruitment of Glc7 for SAC silencing via the RVSF motif of Spc105 should be minimized to ensure the formation bipolar attachments. Phosphorylation is a strong candidate mechanism for achieving temporal regulation of Glc7 recruitment. Therefore, we scanned the mass spectrometry database for residues proximal to the basic patch of Spc105 that are known to be phosphorylated (Craig et al., 2004). We replaced the phosphorylatable residues (marked with an asterisk in Fig. 4F) with negatively charged residues, with the expectation that these mutations would reduce with Glc7 recruitment/activity by interfering with any electrostatic charge-mediated action of the basic patch (Figure 4G and S3C). The phosphomimetic allele also suppressed the benomyl sensitivity of *sgo1Δ* strains. Thus, the

phosphorylation of Spc105 by mitotic kinases will suppress Glc7 recruitment to ensure that error correction occurs with maximal effectiveness. It is difficult to clearly identify either Mps1 or Ipl1 as the specific kinase responsible for this phosphoregulation, because both are active at the same time and place. Nonetheless, this experiment underscores the importance of regulated of Glc7-Spc105 interaction for effective error correction.

Artificial loading of PP1 on Spc105 demonstrates the necessity of timely PP1 recruitment for accurate chromosome segregation

As the final validation of our conclusion that Glc7 recruitment via Spc105 must be delayed until the completion of error correction, we used rapamycin-induced dimerization of the Fkbp12 and Frb domains to artificially load Glc7 on Spc105 at a chosen time during mitosis (Haruki et al., 2008). To mimic the position of Glc7 recruitment via the RVSF motif, we fused Frb to the N-terminus of Spc105, and Fkbp12 to the C-terminus of Glc7. Moreover, we constructed the strain such that the cells expressed both Spc105 and Frb-Spc105 so as to reduce the amount of Glc7 loaded in kinetochores.

We first studied the effect of premature Glc7 recruitment on kinetochore biorientation (work flow depicted at the top of Fig. 5A). For this, we first arrested cells in mitosis by treating them with nocodazole, and then loaded Glc7 onto Spc105 by treating the cells with rapamycin. We found that Bub3 recruitment to unattached kinetochores remained unchanged even after rapamycin treatment (Fig. S3D). We released these cells from the metaphase block by washing out nocodazole, and examined kinetochore biorientation 30 minutes after the release. In 30 minutes, the majority of untreated cells formed normal spindles with bioriented kinetochore clusters (Fig. 5A, left). In contrast, most rapamycin-treated cells showed abnormal spindle morphology (Fig. 5A, bar graph). The defects include: (1) unequal distribution of kinetochores between the two spindle pole bodies (quantified by calculating the absolute difference between the normalized intensity of the brightest pixel in each spindle half), (2) unaligned kinetochores along the spindle axis, (3) reduced separation between kinetochore clusters and spindle pole bodies (0.43±.11 vs. 0.27±18 μm mean ± s.e.m.), and (4) abnormally long spindles (scatterplots in Fig. 5A and S3E). The unequal distribution of kinetochores between the two spindle pole bodies is a hallmark of defective biorientation (Marco et al., 2013). Smaller number of bioriented sister kinetochore pairs also result in a reduced centromeric tension, which leads to increased spindle length (Bouck and Bloom, 2007).

We next studied the effects of artificial Glc7 loading on Spc105 after the process of kinetochore biorientation is complete (Fig. 5B, schematic at the top). For this, we first repressed *CDC20* expression to block anaphase onset and enable sister kinetochores sufficient time to form bipolar attachments. After ensuring biorientation, we added rapamycin to load Glc7 at the N-terminus of Spc105. In this case, artificial Glc7 loading had no discernible phenotype (scatterplots in Fig. 5B): the spindle morphology was nearly identical with or without rapamycin-treatment with the exception of a small decrease in spindle length. Kinetochores were also distributed symmetrically in two distinct clusters. Thus, Glc7 loading after kinetochore biorientation does not adversely affect kinetochore-microtubule attachment.

Interestingly, the nature of Spc105 N-terminus as a flexible, unstructured domain likely plays a role in the observed phenotypes (Aravamudhan et al., 2015). Using the same methodology, we artificially loaded Glc7 at the C-terminus of Ndc80. The C-terminus of the Ndc80 complex is located at the same average position in the yeast kinetochore as the N-terminus of Spc105, but it is unlikely to possess the same degree of freedom of movement within the inner kinetochore as the Spc105 N-terminus (Aravamudhan et al., 2015; Joglekar et al., 2013b; Joglekar et al., 2009). In keeping with the previous experiment, we conducted these experiments in heterozygous diploid cells expressing both Ndc80 and Ndc80-Fkbp. Interestingly, premature Glc7 loading at the Ndc80 C-terminus had no observable adverse effects on sister kinetochore biorientation, spindle morphology, or cell cycle progression (Fig. 5C). The likely explanation for the lack of a phenotype in this experiment is that the Glc7 attached to the Ndc80 C-terminus is unable to access its targets (Dam1 complex subunits and Ndc80 N-terminus). Therefore, despite being recruited to the kinetochore prematurely, this Glc7 cannot contribute to the stabilization of kinetochore-microtubule attachments.

The molecular mechanisms of SAC signaling, force generation, and error correction are built around a set of core kinetochore components located in close proximity (Aravamudhan et al., 2014; Aravamudhan et al., 2015). These components are regulated by some of the same enzyme including PP1. Therefore, the possibility of inadvertent cross-talk in the regulation of kinetochore proteins must be considered as a significant issue for kinetochore function. We demonstrate a deleterious cross-talk between SAC silencing and error correction resulting from the involvement of Glc7 in both the processes. We find that Glc7 activity required for error correction and SAC silencing is derived from independent sources. Glc7 needed for SAC silencing is recruited by the conserved RVSF motif and basic patch in Spc105 patch acting together. The source of Glc7 activity used in error correction is unclear. It may be derived from

diffusive interactions between Glc7 and kinetochore proteins involved in force generation. A dedicated Glc7 recruitment mechanism may not even be necessary, because the inter-centromeric tension generated by sister kinetochores can also stabilize bipolar attachments (Akiyoshi et al., 2010; Franck et al., 2007). Importantly, the improved chromosome biorientation in cells expressing Spc105^{BPM} or Spc105^{RASA}, and the extensive positive genetic interactions between *SPC105*^{BPM} and mutations in factors involved in error correction strongly suggest that the suppression of Glc7 recruitment via Spc105 is crucial for the formation of bipolar attachments. It is likely achieved by the phosphorylation of Glc7 binding motifs in Spc105 including the basic patch, which will disrupt Glc7 recruitment. Thus, the use of separate Glc7 sources and the suppression of Glc7 recruitment for SAC silencing will together ensure that SAC silencing occurs only after bipolar attachments are formed (Fig. 5D, left panel). Our artificial Glc7 loading experiments demonstrate the cell biological significance of orchestrating kinetochore biorientation before SAC silencing.

Sequential execution of error correction and SAC silencing is also likely to be crucial in the human kinetochore. Even though the two processes are executed by a much more complex and overlapping network of three kinases (Fig. 5D, right panel), their targets include KNL1 and many of the same kinetochore proteins (Etemad et al., 2015; Hiruma et al., 2015; London et al., 2012; Nijenhuis et al., 2014; Suijkerbuijk et al., 2012). Aurora B regulates PP1 recruitment by phosphorylating both, the RVSF motif and the SILK motif, which interestingly, lies directly adjacent to a basic patch (Liu et al., 2010; Welburn et al., 2010). PP1 recruitment in the human kinetochore also peaks only after kinetochores establish bipolar attachments (Liu et al., 2010). Our findings suggest a new model (Fig. 5D, right panel), wherein Aurora B suppresses PP1 recruitment by KNL1 mainly to ensure that error correction is completed before PP1-mediated stabilization of bipolar attachments and SAC silencing takes place.

Acknowledgements

This work was funded by the RO1-GM-088908 to APJ. We would like to thank Mara Duncan for sharing reagents. We thank Sue Biggins, members of the Joglekar lab, and the Duncan lab for their support and constructive comments.

Methods

Plasmid and Strain construction: Budding yeast strains and plasmids utilized in this study are listed in Supplementary Tables S1 and S2 respectively. Strains containing multiple genetic modifications were constructed using standard yeast genetics. GFP(S65T) and mCherry tagged to proteins were used to localize kinetochores by microscopy. The C- terminal tags and gene deletion cassettes were introduced at the endogenous locus through homologous recombination of PCR amplicons (Jürg Bähler et al., 1998). A 7-amino-acid linker (sequence: 'RIPGLIN') separates the tag (GFP, mCherry) from the C-terminus of the tagged-protein. We have previously observed that the intensity of mCherry-tagged kinetochore proteins varies significantly from strain to strain due to inherent variability of the brightness of mCherry. Therefore, we created all Bub3-mCherry and Mad1-mCherry strains by crossing a specific transformant of the Bub3-mCherry or Mad1-mCherry with strains expressing wild-type Spc105 or its mutants. Mad1-mCherry is always accompanied with *nup60*Δ to prevent it from localizing to the nuclear envelopes (Scott et al., 2005). Spc105 chimeras contain a 397 bp upstream and a 250 bp downstream sequence as promoter (*prSPC105*) and terminator (*trSPC105*) respectively. To build haploid strains expressing $Spc105^{222::GFP}$ alleles (wild-type or mutant with GFP inserted at amino acid 222), first, we deleted a wild-type genomic copy of *SPC105* in a diploid strain of YEF473 to form the strain AJY3278 *(SPC105/spc105Δ::NAT1)*. Then we transformed this strain with the chimeras with pRS305, after linearizing the plasmid with *Bst*EII. We sporulated the correct transformants to obtain Nourseothricin resistant and Leucine prototroph segregants. We linearized the plasmids based on pRS306 by *Stu*I before transformation. To visualize centromere 4 segregation, first we built a diploid strain which is homozygous for *CENIV-tetO*, *tetR*-GFP, and *SPC29*-mCherry but heterozygous for *SPC105* (AJY5160). We digested pAJ817 (WT) and pAJ818 (BPM) by *Sac*II-*Kpn*I before transforming them in this strain. After that we sporulated the correct transformants to obtain the haploid strains.

We obtained the pSB148 from Biggins lab. In this plasmid, *IPL1* ORF is flanked by 1.0 Kb upstream as promoter (*prIPL1*) and 654 bp downstream sequence as terminator (*trIPL1*). We performed site directed mutagenesis with the Quick change kit (Agilant Technologies) to introduce the *ipl1-2* (H352Y) mutation in the *IPL1* ORF. We acquired *sgo1*Δ and *rts1*Δ from the yeast deletion library (Giaever et al., 2002). The strains with *sgo1*Δ demonstrated variable growth. Hence, we backcrossed them with YEF473 to remove any background mutations. We tested both normal and slow growing segregants for growth assays on YPD and YPD+Benomyl.

We confirmed the strains with bub1ΔK (kinase deleted bub1) by western blot by anti-mCherry antibody and localization at unattached kinetochores.

To build the strains containing *ndc80-6A* or *dam1-3A*, first we deleted one allele of *NDC80* or *DAM1* ORF with *TRP1* marker. Next, we replaced the deleted allele with ndc80-6A (*KAN*) or dam1-3A (*KAN*) by transforming the transforming the heterozygous deletion strains of *NDC80* and *DAM1* with *Sac*II-*Apa*I digest of pAJ108 (ndc80-6A) and *Sac*II-*Sma*I digest of pSB617 (dam1-3A) respectively. After confirming the integration of the cassettes, we sporulated the diploids to obtain tryptophan auxotroph and G418 resistant segregants. We also confirmed the haploid strains with *ndc80-6A* and *dam1-3A* by colony check PCR followed by Sanger sequencing.

To construct the plasmids containing 6XHIS-MBP-Spc105$^{2\text{-}455,\ 222::GFP}$, we used a pET28a chimera where MBP is already cloned within *Nhe*I-*Bam*HI sites. 6XHIS and MBP are separated by a linker of 13 amino acids (SSGLVPRGSHMAS) and a TEV protease cleavage site is present at the downstream of MBP. We cloned fragments containing SPC105$^{2\text{-}455,\ 222::GFP}$ of WT, BPM or RASA within *Sal*I-*Eag*I sites, that are present at the downstream of MBP-TEV. Hence translation of the whole chimera will result into expression of a 1123 amino acids long protein in which 6XHIS-MBP-TEV is linked with the phosphodomain by a 9 amino acids long peptide fragment (GSEFELRRP).

Cell culture: We grew yeast strains in YPD (yeast extract 1%, peptone 2%, dextrose 2%) at room temperature (25°C) and 32°C. They were imaged in room temperature in presence of synthetic dextrose media, supplemented with essential amino acids. We added Nocodazole and methionine to the mounting media to image the nocodazole arrested cells and Cdc20 depleted cells respectively. To form zygotes for constructing diploid strains, we mixed overnight grown cultures of two strains of opposite mating types and spotted on YPD plate which was incubated for 3-4 hours at 32°C. To induce sporulation, we grew diploid yeast cells were grown in YPD overnight to stationary phase. Then the cells were pelleted down and resuspended with starvation media (yeast extract 0.1%, Potassium acetate 1%) and incubated 4-5 days at RT.

Metaphase arrest by Cdc20 depletion: We synchronized the strains expressing Cdc20 from *prMET3* by treating them with α factor (2μg/ml) for 2 h in synthetic dextrose media lacking methionine. After that, they were washed to remove α factors and released in YPD supplemented with 2M methionine to knock down Cdc20 expression for 1-2 h. To release from

Cdc20 repression mediated metaphase arrest, we washed the cells with synthetic media lacking methionine and incubated them in the same.

Treatment of cells to study spindle pole and centromere 4 separation: For this experiment, we used strains with TetO-CENIV, TetR-GFP, and Spc29-mCherry. We synchronized them at G1 stage with α factors (2 µg/ml) for 1h 45 min. They were then washed and released in Nocodazole supplemented (15 µg/ml) media to disrupt the spindle and activate the spindle checkpoint for 2 h. After that, we again washed them to remove Nocodazole and release them in fresh YPD. Cell samples were collected and imaged at 0, 30 and 45 mins.

Benomyl sensitivity assay: We prepared 10-fold serial dilutions of log-phase cultures starting from 0.1 OD_{600} and frogged on YPD or YPD containing 20 and /or 30 µg/ml benomyl (YPD+Ben^{20} and YPD+Ben^{30} respectively). Plates were incubated at 32°C and plate images were taken after 2 (on YPD) or 3 (YPD+Benomyl) days. All benomyl spotting assays were performed with at least two biological wherever possible and two technical replicates on both YPD+Ben^{20} and YPD+Ben^{30}. However, for space limitation only one of benomyl plate images has been mentioned in the figures. In every spotting assay with benomyl plates of fig. 1, 2, 3, 4, 1S and 2S we included the strain of $Spc105^{222::GFP}$ (wild type or WT) as positive control and *mad2*Δ or spc105-6A (inactive MELT repeats) or *sgo1*Δ as negative control.

Microscopy and image acquisition and analyses: A Nikon Ti-E inverted microscope with a 1.4 NA, 100X, oil-immersion objective was used in microscopy (Joglekar et al., 2013a). A ten-plane Z-stack was acquired (200nm separation between adjacent planes). To measure Bub3 and Mad1-mCherry, the 1.5x opto-var lens was used. Total fluorescence of kinetochore clusters (16 kinetochores in metaphase) was measured by integrating the intensities over a 6x6 region centered on the maximum intensity pixel. The median intensity of pixels immediately surrounding the 6x6 area was used to correct for background fluorescence. The calculations were performed using ImageJ or semi-automated MATLAB programs as described earlier (Joglekar et al., 2006).

Analysis of kinetochore biorientation was conducted using a MATLAB GUI according to the scheme developed previously (Marco et al., 2013). Briefly, a region of interest containing the two spindle poles were manually selected from each cell. The script then identified the locations of the spindle poles and rotated the image so that the spindle axis (defined by the two spindle poles) coincides with the horizontal axis. Next, the fluorescence intensity in the GFP channel (used to record $Spc105^{222::GFP}$) over a rectangular region centered on the spindle axis and

extending 4 pixels on either side of the spindle axis was summed to define the kinetochore distribution at each pixel along the spindle axis. The kinetochore distribution was then normalized by the total fluorescence to obtain the fluorescence line scan for each cell. Line-scans from > 50 cells were then displayed as a heat map in Figures 1 and 3. G1-arrested yeast cells expressing either wild-type Spc105 or Spc105^{BPM} were released into the cell cycle, and the distribution of kinetochores along the spindle axis (defined by the locations of the two spindle poles) was analyzed at 15-minute time intervals and visualized as a heat-map. Because yeast cells enter mitosis after ~ 30 minutes following release from a G1 arrest, only 45 and 50-minute time points shown in Fig. 1. In this visualization, each pixel row represents the kinetochore fluorescence line scan for a single cell, with the pixel rows have been sorted according to spindle length (longest to shortest from top to bottom, > 50 cells for each cell for each time-point).

Quantitative assessment of the relative distribution of kinetochores in the two spindle halves was obtained on the basis of the normalized kinetochore distribution as calculated above. Briefly, the brightest pixel in each spindle half was identified from the fluorescence line scan, and the absolute value of the intensity difference between these pixels was used as the measure of asymmetry in kinetochore distribution.

Flow cytometry: We performed flow cytometry as described previously (Baum and Clarke, 2000). Starting from overnight inoculum, we grew the yeast strains to mid log phase. Then we added Nocodazole (final concentration 15µg/ml) to the cultures to depolymerize spindle and activate the spindle checkpoint (Gillett et al., 2004). We collected the cell samples of 0.1 OD_{600} at designated time points (0, 1, 2 and 3 h).

Spc105 phosphodomain Purification: The 6XHIS-MBP-Spc105$^{2\text{-}455,\ 222::GFP}$ fusion construct was expressed in BL21-Rosetta 2 (DE3) (Novagen) or T7 expression *E. coli* cells (NEB) using 0.25 mM IPTG for 16 hours at 18 °C. Cells were then harvested, and resuspended in the lysis buffer (20 mM Tris (pH 7.5), 300 mM NaCl, 5 mM Imidazole, 0.1% TritonX-100 (Sigma), 5% glycerol, 1 mM PMSF) supplemented with complete EDTA-free protease inhibitor mix (Roche). Cells were lysed by sonication (3X for 3 minutes with 30 second pulse on and 30 second pulse off). Cleared supernatant was incubated with Ni-NTA agarose beads (Invitrogen) for 2 h at 4°C. Beads were washed with lysis buffer containing 500mM NaCl and 30mM Imidazole, and protein was eluted with lysis buffer containing 150mM NaCl and 250mM Imidazole. Subsequently, the protein was loaded onto a 16/60 Superdex 200 size exclusion column (GE) equilibrated with gel filtration buffer (20 mM Tris pH 7.5, 100 mM NaCl, 5% glycerol, and 1 mM DTT). Fractions were

analyzed by SDS-PAGE and Coomassie staining, and peak fractions were aliquoted and stored at −80 °C.

Preparation of X-rhodamie labeled microtubules: X-rhodamine (Cytoskeleton) labeled microtubule was achieved by using a mixture of X-rhodamine (1.25mg/ml) and unlabeled tubulins(10mg/ml) in BRB80 buffer (80 mM PIPES/KOH, pH 6.8, 1 mM $MgCl_2$, 1 mM EGTA) containing 1 mM GTP and 4 mM $MgCl_2$ at 37 °C. Microtubules were further stabilized by the addition of 10 μM Taxol and incubation at 37 °C for 15 min. Microtubules were pelleted down by ultracentrifugation (55,000 rpm for 10 minutes at 37°C) to get rid of unpolymerized tubulin.

Decoration of Polystyrene beads with recombinant Spc105 phosphodomain: The assay was performed as previously described with small modifications (Espeut et al., 2012). In brief, decoration of Spc105 proteins on polystyrene beads was achieved using streptavidin-biotin system. 100 nm of WT and mutant Spc105 proteins was incubated with 10 µl of 0.1% w/v streptavidin polystyrene beads (Spherotech) conjugated with anti-penta-his biotin antibody (Qiagen) for 1 and half hours at 4°C. Before imaging, the beads were sonicated for 3 minutes in a water bath containing ice cubes. Subsequently, the beads were introduced inside the flow chamber coated with taxol stabilized microtubules. The images were acquired using TIRF microscope.

Sample preparation for TIRF imaging: Flow cells were created as described before (Verma et al., 2015). Flow cells were first incubated with 30 µl of 1:100 dilution of monoclonal anti-β-Tubulin antibody (Sigma) for 10 minutes in a humidified chamber, followed by another incubation of 0.5% w/v Pluronic F-127 (Sigma) for 10 minutes, and 30 µl of X-rhodamine labeled microtubule for 20 minutes. The flow cells were then incubated with 30 µl of 2.5mg/ml casein for 5 minutes to block nonspecific sites. After blocking, flow cells were incubated with 30 µl of polystyrene beads decorated with WT or mutant Spc105 proteins and scavenging system (40 nM $_D$-glucose, 250nM glucose oxidase, 64nM catalase and 1% (v/v) β-mercaptoethanol in BRB80 containing 50 mM NaCl (80 mM PIPES, 1 mM $MgCl_2$, 1 mM EGTA, 50mM NaCl, pH 6.8). Subsequently, chambers were sealed, and samples were immediately imaged using TIRF microscope.

TIRF microscopy: All images were acquired as described before (Verma V et. al, Plos one, 2015) with little modifications. In brief, Images were acquired on a Nikon Ti-E microscope equipped with a 100X 1.4 NA CFI-Apo oil immersion objective, an EMCCD camera (iXon+ DU 897; Andor), a 3 line (488, 561 and 640nm) monolithic laser combiner with AOTF laser system

(Agilent) and Nikon NIS-Elements software. Images of X-rhodamine labeled tubulin and Spc105-GFP were acquired at the following settings: 600 frames @ 50ms exposure time, conversion gain-1X, EM multiplier gain setting 288, 561 laser power-40% and 488 laser power-40%. For TIRF image analysis, length of the microtubule was calculated with the help of Fiji software, and intensity of the Spc105-GFP conjugated with streptavidin polystyrene beads was measured using a custom built software in MATLAB as described before (Joglekar et al., 2006).

GFP-trap assay: We performed GFP-TRAP experiments using the GFP-TRAP-A beads (Chromotek #gta-20). We dialyzed the Ni-NTA elutes of 6XHIS-MBP fusion proteins of WT, BPM, ∆80-128 and RASA phosphodomains with 1X buffer A (10mM Tris-Cl pH7.5, 150 mM NaCl, 0.5mM EDTA, 1mM DTT). We prepared total cell lysate from cells expressing Glc7-13xMyc in the same buffer using liquid nitrogen lysis. We incubated the beads with same amount of proteins at 4°C for 1h. Then after washing the supernatants, we re-incubated them the Glc7-13xMyc cell lysate at 4°C for 1h. After that, we washed the beads with 1X buffer A and resuspended them in 1X SDS-PAGE loading buffer. They were boiled immediately and loaded in 10% SDS-PAGE gel to probe with Mouse α-GFP (1:2000) and Mouse α-MYC (1:3000). The bands obtained after exposure with chemiluminescent substrates, were analyzed by ImageJ program for intensity calculation.

Artificial loading of Glc7: For these set of experiments, we used the yeast strains where Glc7-Fkbp can be loaded on N-termini of Spc105 (FRB-GFP-Spc105) or Glc7-Frb-GFP can be loaded at Ndc80-C termini (Ndc80-Fkbp12) by adding rapamycin to the culture. To investigate Glc7 loading in prophase, haploid strains of were arrested in G1 by α factor treatment (2 µg/ml) for 1h 45 min. They were then washed and released in YPD media. 30 min after release from the G1 arrest (time at which cells are in S-phase with duplicated spindle pole bodies, and are in the process of kinetochore biorientation), we added nocodazole to the media (15 µg/ml) to disrupt the spindle structure and activate the spindle assembly checkpoint. After 30 min., the cells were washed again to remove nocodazole, and released in Rapamycin supplemented growth media for 30mins before imaging. To load Glc7 in metaphase, we repressed *CDC20* expression for 1h 10min. Then we supplemented the media with rapamycin and incubated for 30min before imaging.

To examine the loading of Glc7 at Ndc80-C termini in prophase, we used the diploid strains. These strains were first arrested in S/G2 by hydroxyurea (100mM). The cells were then washed and released into growth media containing nocodazole. After incubation with nocodazole for 45

min, we washed the cells again and resuspended them in growth media, supplemented with rapamycin for 30min, before processing the cells for imaging.

Figures

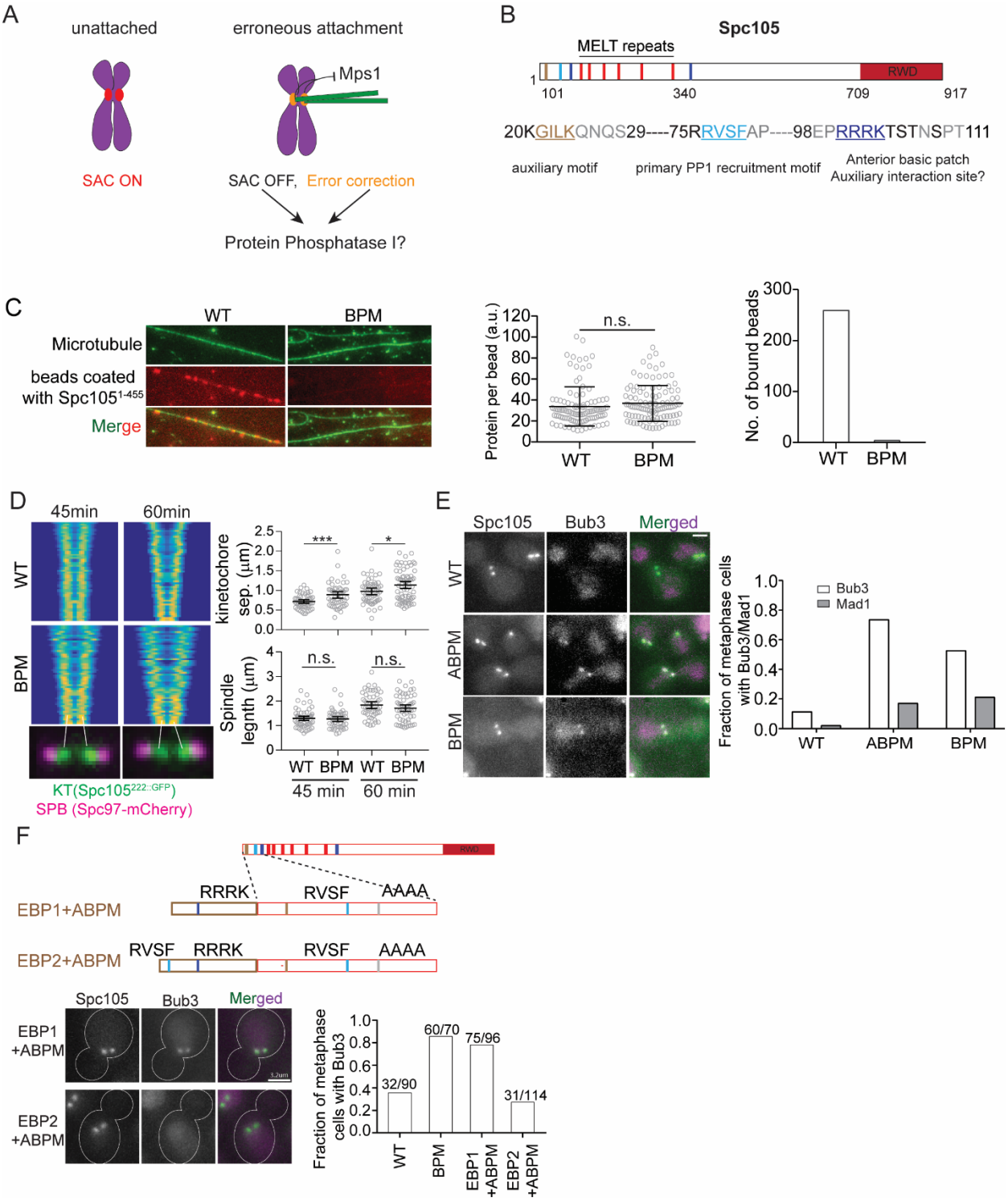

Figure 1. A conserved basic patch near the N-terminus of Spc105 contributes to Glc7 recruitment. (A) Overlapping regulation of two kinetochore functions by PP1. **(B)** Functional

domains of Spc105 and the amino acid sequence of its N-terminus. **(C)** Left panel: Total Internal Reflection Fluorescence micrographs showing the interaction of polystyrene beads coated with recombinant Spc105 phosphodomain (red, amino acid residues 1-455, containing either wild-type or mutant basic patches) with X-rhodamine labelled, taxol-stabilized microtubules (green). Middle panel: Quantification of the average amount of protein conjugated per bead (n = 108 from 2 experiments, p=0.24 using the unpaired t-test). Right panel: Number of interactions observed for the respective phosphodomain (n = 259 and 4 for WT and BPM respectively from 2 experiments). **(D)** Left panel: V-plots display normalized distribution of kinetochores along the spindle axis for the indicated strains (n > 50 for each time point). Each row of pixels in the plot represents the symmetrized distribution of $Spc105^{222::GFP}$ or $Spc105^{BPM\text{-}222::GFP}$ along the spindle axis in one cell. Rows are ranked according to spindle length (see methods and ref. (Marco et al., 2013)). Right top scatterplot: Average sister kinetochore separation (p=0.0005 and 0.0121 for 45 and 60 min respectively using the unpaired t-test). Right bottom panel: distance between two spindle poles (p=0.6523 and 0.1932 for 45 and 60 min respectively using the unpaired t-test). **(E)** Top panel: representative micrographs of yeast cells expressing the indicated Spc105 variant. Bottom panels: Frequency of metaphase cells with visible Bub3 and Mad1 at the kinetochores (n = 204, 196 and 179 respectively pooled from 2 experiments for Bub3-mCherry recruitment, and n= 101, 94 and 123 for Mad1-mCherry recruitment). Scale bar~3.2µm. **(F)** Representative micrographs show Bub3 recruitment in cells expressing two versions of Spc105 displayed in the cartoons at the top. Bar graph: Fraction of cells with visible Bub3-mCherry recruitment (n = 90, 70, 96 and 114 for respectively pooled from 2 experiments). Scale bar~3.2µm.

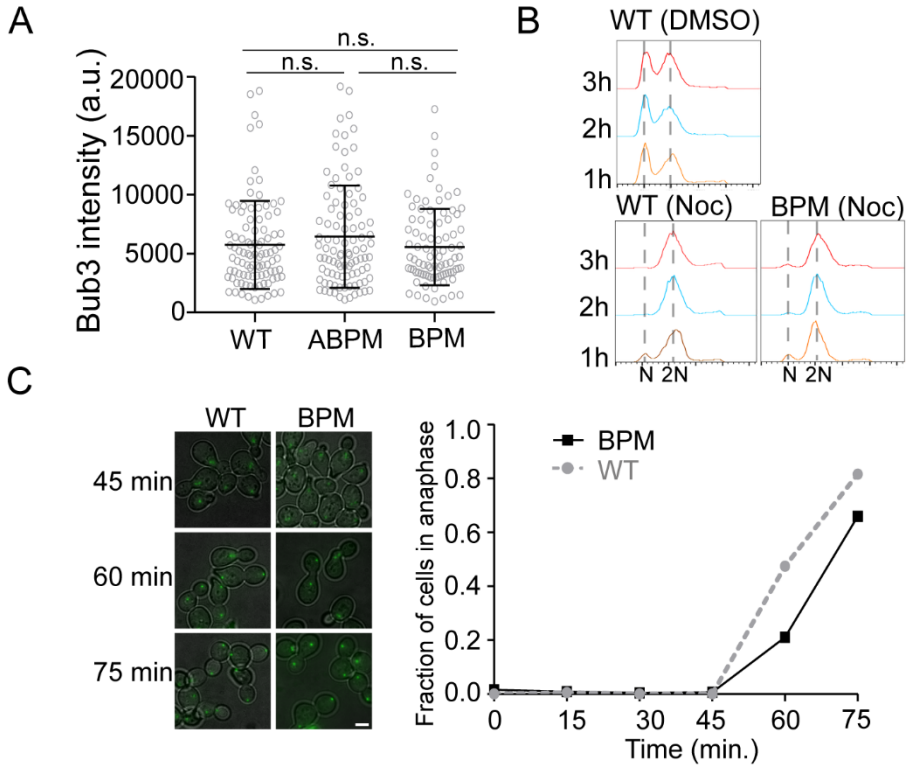

Figure 2. Spc105^{BPM} does not enhance SAC signaling, but enhances the error correction mechanism in an Sgo1-independent manner. (A) Recruitment of Bub3 by unattached kinetochores in strains expressing the indicated Spc105 variant (mean ± s.d.; p=0.2501 obtained from one-way ANOVA test, n = 97, 97, and 88 respectively pooled from 2 experiments). **(B)** Flow cytometry of the DNA content per from cultures treated with Nocodazole. The 1n and 2n peaks correspond to G1 and G2/M cell populations respectively (representative histograms from 2 trials). **(C)** Cell cycle progression of cells from G1 to anaphase analyzed by counting the fraction of cells expressing either wild-type Spc105 or Spc105^{BPM} in early or late anaphase (data from pooled from two trials). Scale bar~2.0µm.

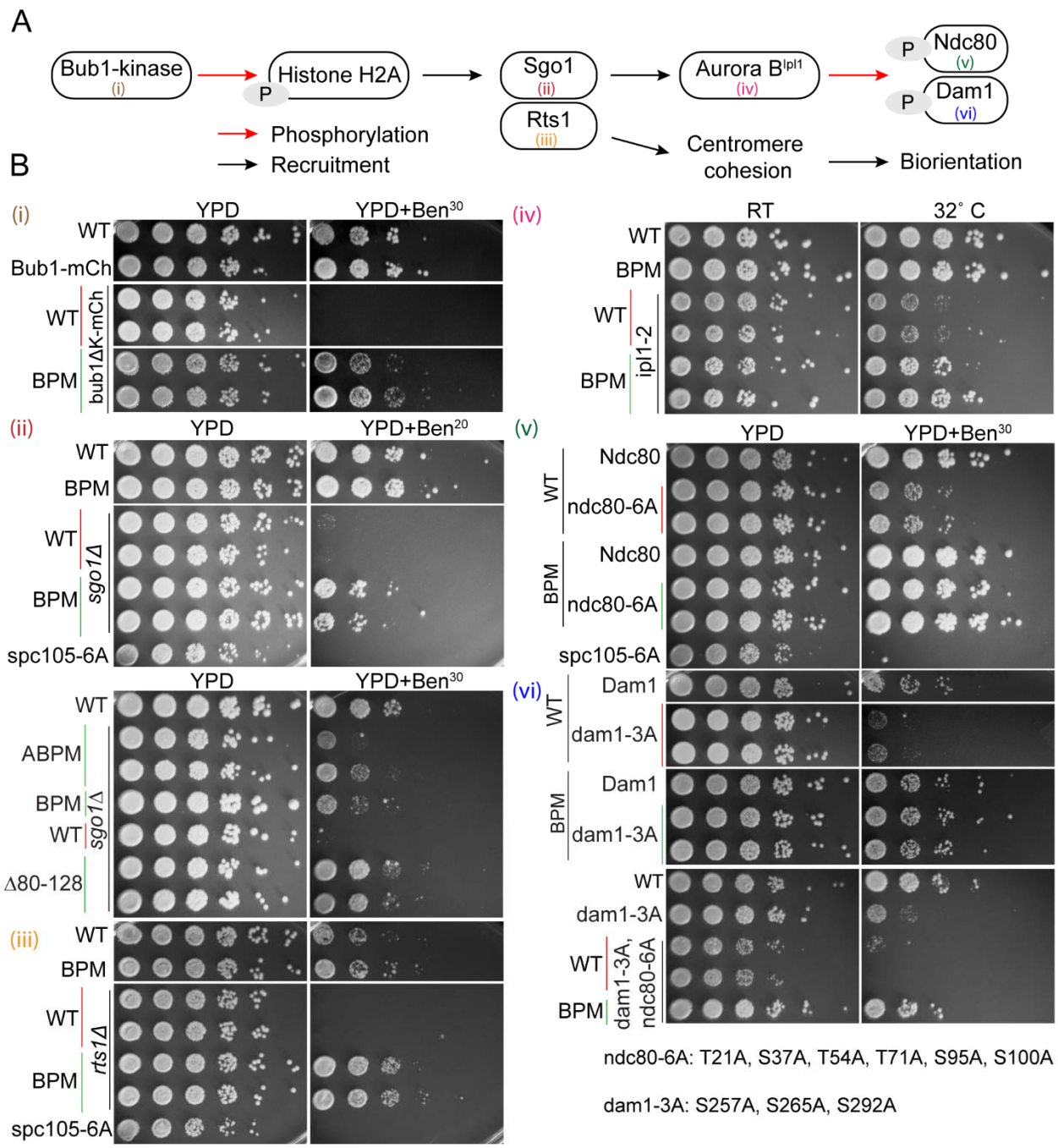

Figure 3. Spc105^{BPM} improves the error correction pathway independently of Sgo1. (A) Schematic of the sister centromere cohesion and biorientation pathway in budding yeast. **(B)** Serial dilutions of yeast cells spotted on either rich media or media containing either 20 or 30 µg/ml Benomyl, a microtubule destabilizing drug. WT at the top of each plating indicates wild-type strain included as a positive control. WT, BPM, or ABPM in other rows refers to the Spc105

allele. *spc105-6A,* wherein all six MELT motifs are rendered non-phosphorylatable, was used as the negative control.

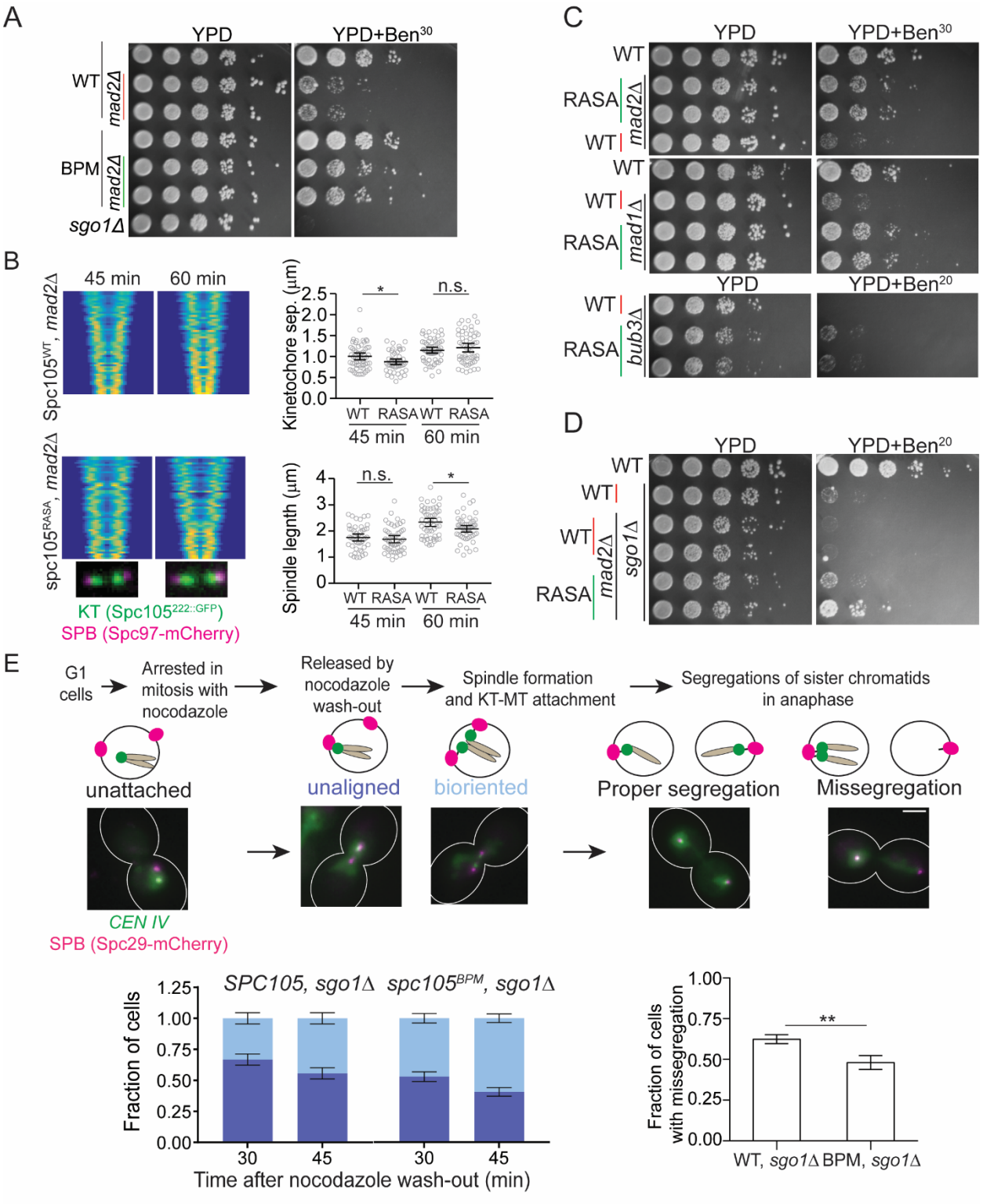
A
YPD
YPD+Ben30
WT
mad2Δ
BPM
mad2Δ
sgo1Δ
B
45 min
60 min
Spc105WT, mad2Δ
spc105RASA, mad2Δ
KT (Spc105222::GFP)
SPB (Spc97-mCherry)
Kinetochore sep. (µm)
Spindle legnth (µm)
n.s.
*
WT RASA WT RASA
45 min 60 min
C
YPD
YPD+Ben30
YPD+Ben20
WT
RASA
mad2Δ
mad1Δ
bub3Δ
D
YPD
YPD+Ben20
sgo1Δ
E
G1 cells
Arrested in mitosis with nocodazole
Released by nocodazole wash-out
Spindle formation and KT-MT attachment
Segregations of sister chromatids in anaphase
unattached
unaligned
bioriented
Proper segregation
Missegregation
CEN IV
SPB (Spc29-mCherry)
SPC105, sgo1Δ spc105BPM, sgo1Δ
Fraction of cells
Time after nocodazole wash-out (min)
Fraction of cells with missegregation
WT, sgo1Δ BPM, sgo1Δ
F
Phosphorylated
Wild-type KGILKQNQS----RRVSF------EPRRRKTSTNSPT
Pmimic KGILKQNQS----RRVSF------EPRRRKEEENEPT
RVDF KGILKQNQS----RRVDF------EPRRRKTSTNSPT
RVDF+Pmimic KGILKQNQS----RRVDF------EPRRRKEEENEPT
G
ABPM
Pmimic
sgo1Δ

Figure 4. Glc7 recruited by the RVSF motif in Spc105 is not required for error correction. (A, C, and D) Benomyl sensitivity of the indicated strains. **(B)** Separation between sister kinetochore clusters in the indicated strains and at the indicated time after release from a G1 arrest (analysis performed as in 1C, >48 cells displayed). Right top panel: separation between two sister kinetochores in metaphase (Unpaired t-test revealed p=0.0191 and 0.3334 for 45 and 60 min respectively). Right bottom panel: distance between two sister SPBs in metaphase (p=0.5056 and 0.0142 for 45 and 60 min respectively, obtained from unpaired t-test). **(E)** Top: experimentation scheme used to study kinetochore biorientation after nocodazole washout. Bottom left: Fraction of cells with unaligned (dark blue) or bioriented (light blue) centromere IV. Bottom right: Fraction of anaphase cells with centromere IV mis-segregation. (n = 434 and 411 respectively pooled from 2 experiments). Unpaired t-test revealed p=0.0079. Two-way ANOVA test for WT vs. BPM revealed p=0.0074 at 30 min, p=0.0038 at 45 min. Scale bar~3.2µm. **(F)** Top: Potential phosphorylatable residues proximal to the basic patch; residues known to be phosphorylated are marked with an asterisk at the top. Bottom two sequences display the mutants used in this study. **(G)** Spotting assay of the indicated Spc105 mutants on benomyl-containing media.

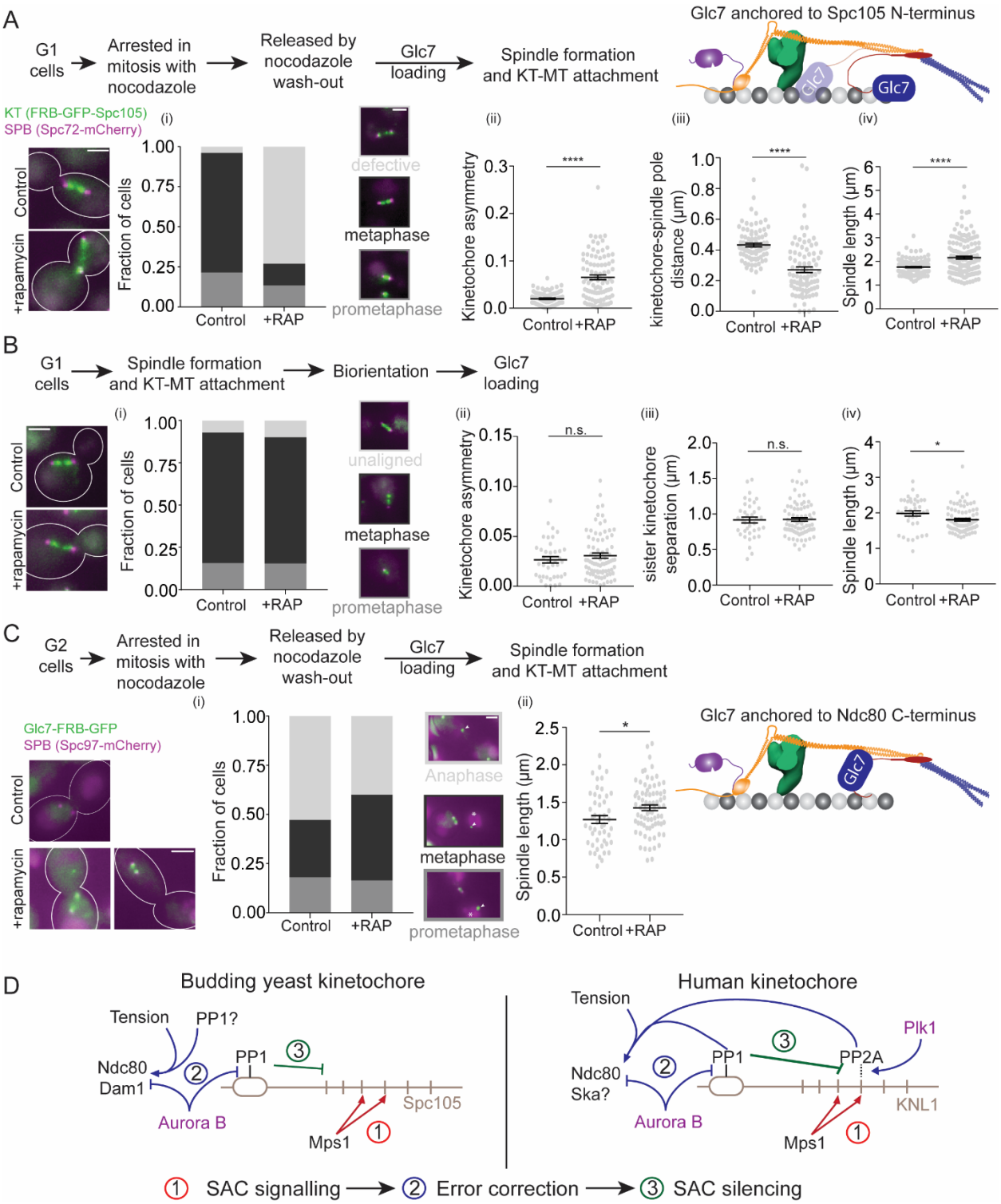

Figure 5. Delayed recruitment of Glc7 for SAC silencing is necessary for the establishment of bipolar chromosome attachment and accurate chromosome segregation. (A) Right: Cartoon depicts the scheme to artificially load Glc7-Fkbp12 near its normal binding site on Frb-Spc105 using the rapamycin-induced dimerization of Fkbp12 and Frb

domains. Note that the Spc105 N-terminus is a flexible and moves throughout the inner kinetochore (Aravamudhan et al., 2015). Left: Flow chart depicts the work-flow to load Glc7 on Spc105 in a prophase-like condition. Bottom left: micrographs depicting the indicated proteins. Scale bar~3.2µm. Bottom right: (i) Bar graph depicts the scoring of cells based on spindle morphology (key provided on the right, n = 126 and 89 for control and rapamycin treated samples respectively, pooled from three technical repeats performed on two biological replicates). (ii-iv) Scatter plots display the indicated quantity in untreated control and rapamycin-treated cells. The data is presented as mean ± s.e.m. (n = 88 and 91 control and rapamycin treated cells respectively, data were pooled from three experimental repeats. $p<0.0001$ with unpaired t-test). (iii) (n = 87 control and rapamycin treated cells pooled from three experimental repeats, $p<0.0001$ using unpaired t-test) (iv) (n = 127 and 153 control and rapamycin treated cells, pooled from three experimental repeats; $p<0.0001$ according to unpaired t-test). **(B)** Flow chart at the top depicts the work-flow for loading Glc7 on the N-terminus of Spc105 in metaphase-arrested cells. Bottom left: micrographs depicting the indicated proteins. Scale bar~3.2µm. Bottom right: (i) Bar graph indicates the scoring of cells based on spindle morphology (key provided on the right; n = 70 and 142 for control and rapamycin treated cells respectively pooled from three technical repeats). (ii-iv) Scatter plots display the indicated quantity in untreated control and rapamycin-treated cells. The data is shown as mean± s.e.m. In (ii), 39 and 80 control and rapamycin treated cells pooled from two experimental repeats; $p=0.3298$, acquired from unpaired t-test. In (iii) and (iv), 38 and 80 cells control and rapamycin treated cells, data pooled from two experimental repeats. In (iii) $p=0.8844$, obtained from unpaired t-test. In (iv) Unpaired t-test showed $p=0.0244$ **(C)** Cartoon at the right depicts the scheme to load Glc7 at the C-terminus of Ndc80 which occupies the same same average position as N-Spc105 ((Joglekar et al., 2009), Roy et al., unpublished data). Left: micrographs depicting the indicated proteins. Note that these are diploid cells. Scale bar~3.2µm. (i) Scoring of cells at prometaphase, metaphase and anaphase stages (n = 138 and 273 for control and rapamycin treated samples respectively). The arrowhead marks cytoplasmic foci of Glc7-FRB-GFP that form in rapamycin-treated samples. The asterisk marks vacuoles, which accumulate auto fluorescent material during the G2 arrest induced by hydroxyurea treatment. (ii) Scatter plot: quantification of spindle length in control and rapamycin treated samples (mean± s.e.m., n = 49 and 76 cells from two experimental repeats, $p=0.0158$ by unpaired t-test). **(D)** Left: Model explaining the mechanism that mitigates harmful cross-talk between the SAC silencing and error correction mechanisms in budding yeast kinetochore. Right: schematic of the proposed

mechanism for the human kinetochore. Dashed line indicates indirect recruitment of PP2A via BubR1.

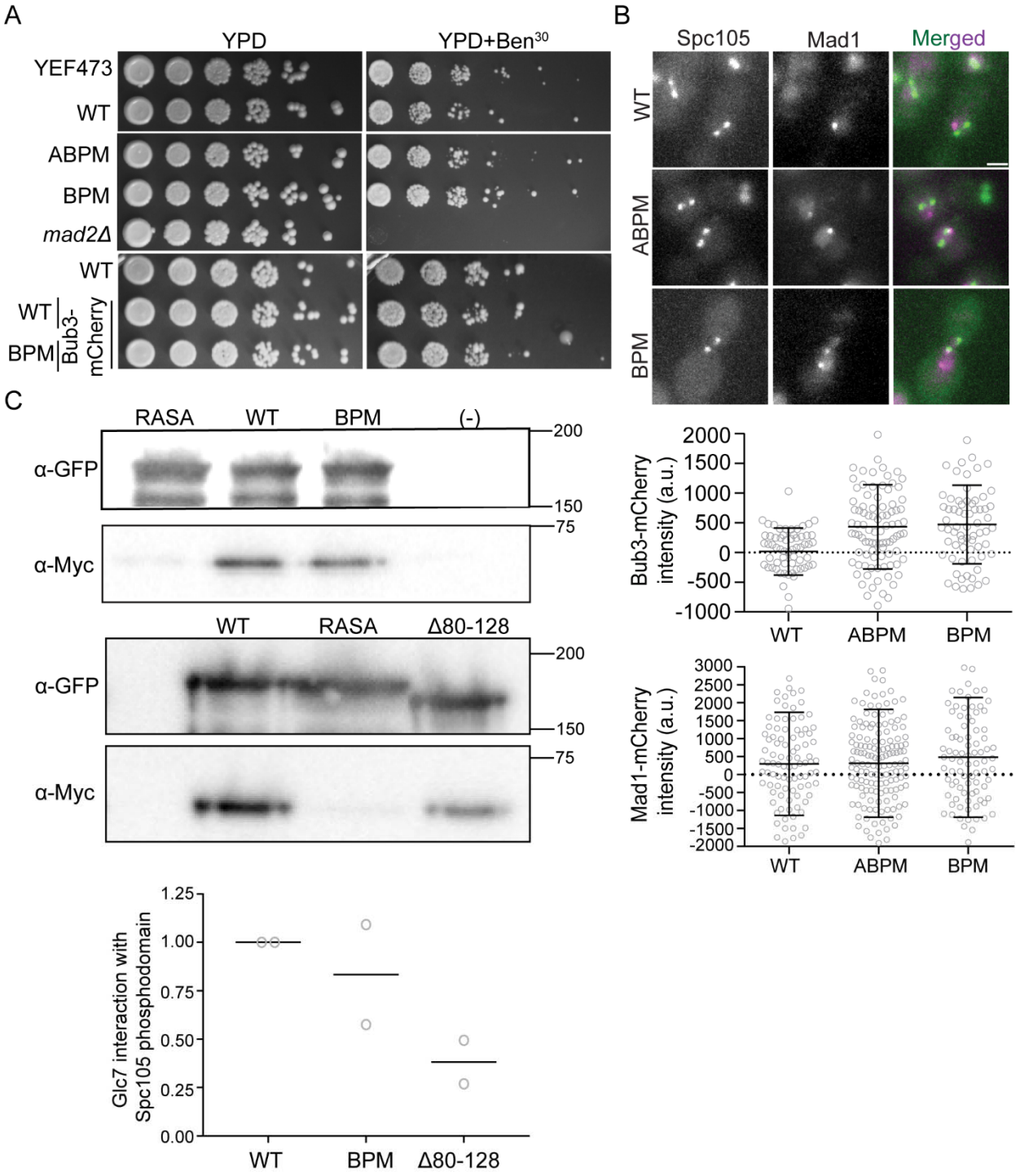

Figure S1. **(A)** Serial dilutions of yeast cells of the indicated genotype on rich media (YPD) and on media containing 30 µg/ml of Benomyl. YEF473 is the parent strain for nearly all the strains constructed in this study. WT refers to a wild-type strain expressing Spc105$^{222:GFP}$ (GFP inserted at amino acid 222 in Spc105). **(B)** Top: representative images of metaphase cells of wild-type, single and double basic patch mutants showing Spc105$^{222::GFP}$ and Mad1-mCherry. Scatter plot:

Quantification of Bub3 and Mad1 recruitment by bioriented kinetochores in metaphase-arrested cells of the indicated genotype. The data are presented as mean+ s.d. (n = 62., 95, 68, for WT, ABPM and BPM respectively pooled from 2 experiments in Bub3-mCherry intensity measurement, and n=103, 165 and 100 for WT, ABPM and BPM respectively pooled from 2 assays in Mad1-mCherry intensity measurement; $p<0.0001$ and 0.1622 for Bub3 and Mad1 respectively using t-test). Scale bar~3.2μm. **(C)** GFP-TRAP assay with 6xHIS-MBP fusion of $Spc105^{222::GFP}$ (WT, BPM and RASA) and Glc7-13xMyc . Top panel: Western blot assay with α-GFP on fraction of WT, BPM and RASA that were bound to the GFP-TRAP beads. Bottom panel: Western blot assay with α-Myc on fraction of Glc7-13xMyc that were co-precipitated with the Spc105 phosphodomain (WT, BPM and RASA) bound to the GFP-TRAP beads. Bottom: Quantification of band intensities of phosphodomains and Glc7-13xMyc by ImageJ (n = 2, horizontal line indicates the mean, normalized intensity). Glc7-13xMyc intensity for the RASA phosphodomains was used as background binding, and subtracted from the other values before normalization with the wild-type intensity (Bottom).

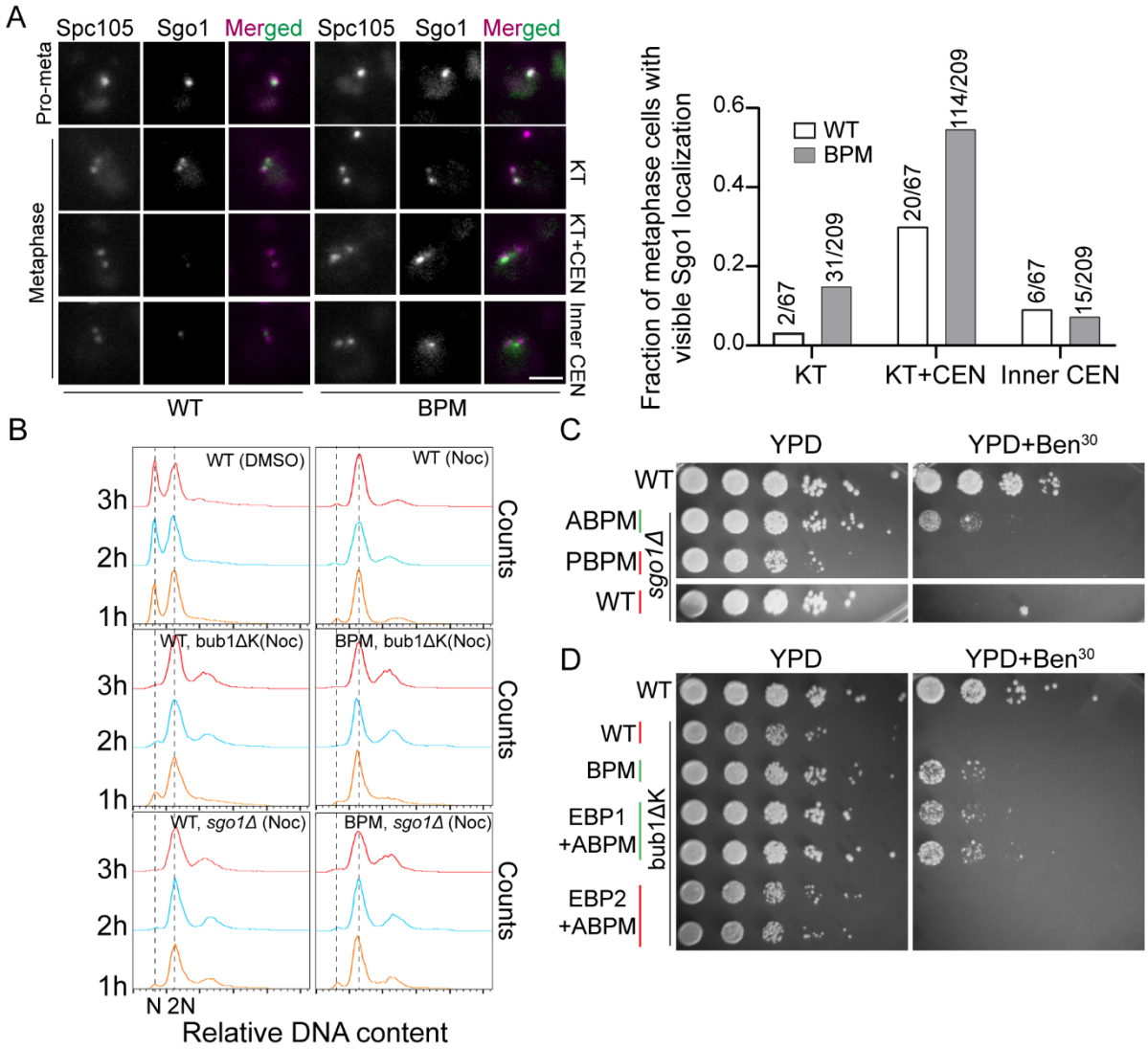

Figure S2. **(A)** Representative micrographs showing the localization of Sgo1-GFP and Spc105$^{222:mCherry}$ in prometaphase (single kinetochore cluster) and metaphase (two distinct kinetochore clusters) cells. The designations used for scoring cell populations is indicated on the right hand side (KT = kinetochore-colocalized, KT+CEN = Sgo1 colocalizes with both kinetochores and the centromeric region in between the two kinetochore clusters, and Inner CEN = Sgo1 localized mainly in the centromeric region, positioned between two sister kinetochore foci). Scoring shown in the bar graph on the right. The numbers mentioned above, represents the number of cells we examined for this assay. (n = 67 and 209 for WT and BPM respectively pooled from 2 experiments). Scale bar~3.2μm. **(B)** Flow cytometry-based verification of competent SAC signaling activity in strains lacking Sgo1 or that express a truncated Bub1 that lacks the kinase domain. **(C)** Benomyl sensitivity of cells lacking sgo1 and expressing an Spc105 variant wherein either the anterior (ABPM) or the posterior basic patch

(PBPM) is mutated to alanine residues. **(D)** Benomyl spotting assay with indicated strains which demonstrates that EBP1 (Spc105$^{79\text{-}145}$) fused to ABPM is not able to revert the effect of ABPM on kinase deleted bub1 (bub1ΔK). In contrast, EBP2 (Spc105$^{56\text{-}145}$, which includes PP1/Glc7 binding RVSF motif) can suppress the effect of mutation of anterior basic patch on bub1ΔK in presence of benomyl.

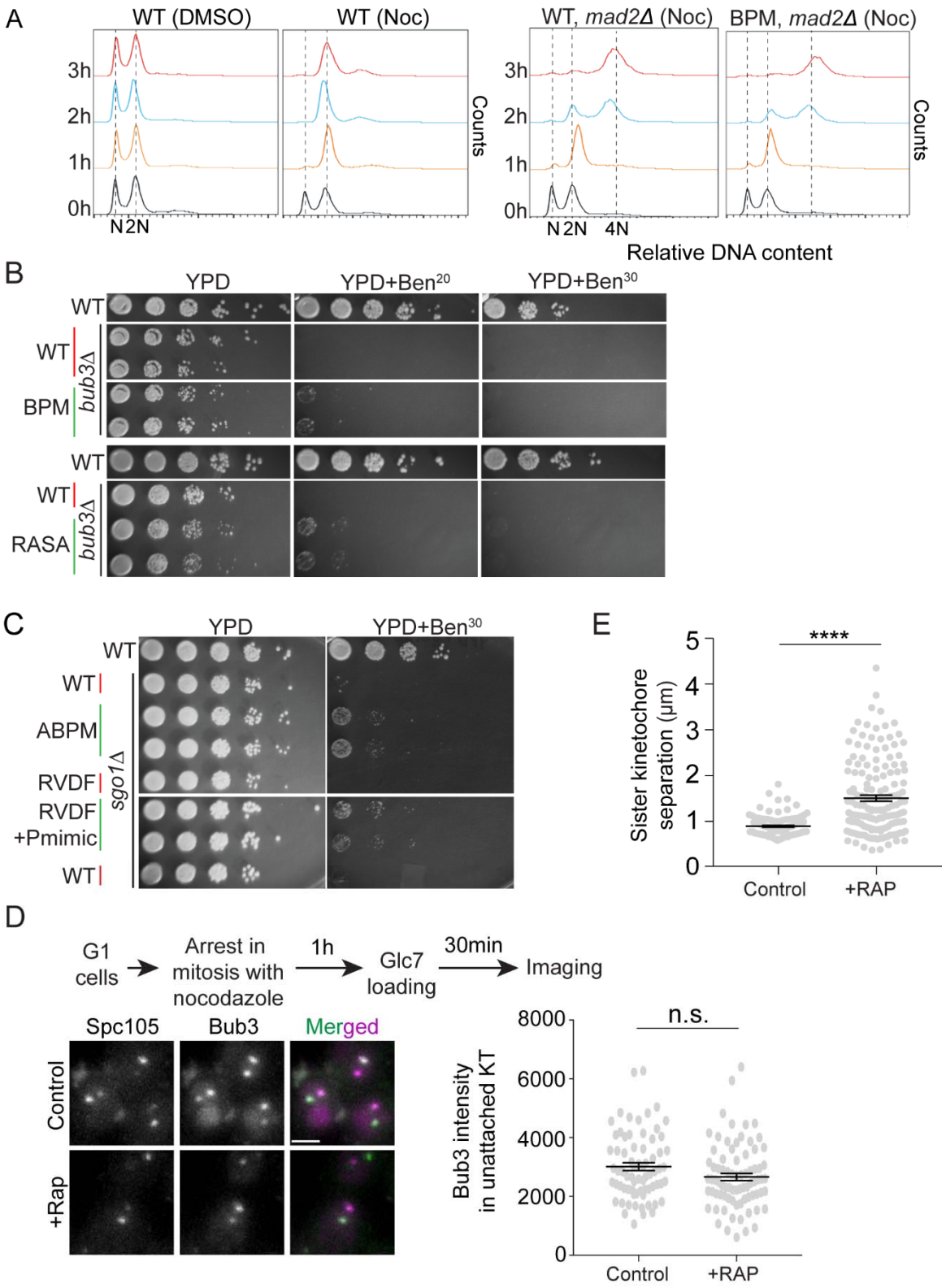

Figure S3: (A) Quantification of DNA content using flow cytometry after activation of the SAC by nocodazole treatment (0h). The first peak in each graph corresponds to cells with 1n DNA

content (G1), whereas the second peak corresponds to cells with 2n DNA content (G2/M). In cells with an inactive SAC (*mad2Δ*), cells fail to arrest in M, and shift to the 4n peak (tetraploid). (**B**) Benomyl spotting assay with indicated strains. Top panel shows that the loss of *BUB3* leads to lethality in media containing even the lower benomyl concentration (20µg/ml). Mutation of basic patch of Spc105 partially suppresses the benomyl sensitivity at the lower, but not the higher concentration of Benomyl (30µg/ml). Bottom panel: Mutation of the RVSF motif of Spc105 leads to suppression of benomyl-sensitivity at the lower, but not the higher, benomyl concentration. **(C)** Spotting assay of the indicated Spc105 mutants on benomyl-containing media. **(D)** Top: Flow chart describes the work-flow to load Glc7 on Spc105 in presence of nocodazole when cells activate SAC in unattached kinetochores. Bottom left: Representative images of FRB-GFP-Spc105, Bub3-mCherry and merged in unattached kinetochores of control and rapamycin treated cells. Scale bar~3.2µm. Bottom right: Scatter plot showing Bub3-mCherry intensities in unattached kinetochores of rapamycin treated and untreated control cells (mean± s.e.m., p=0.0585 obtained from unpaired t-test). The number of kinetochores analyzed for this assay: n = 71 and 78 for control and rapamycin treated cells respectively pooled from 2 experiments performed using two biological replicates. **(E)** Scatter plots display the distance between sister kinetochore foci of untreated and rapamycin-treated cells where Glc7 is artificially loaded in prophase like conditions (n = 124 and 154 cells respectively for control and rapamycin-treated samples obtained from two biological replicates; horizontal lines represent mean± s.e.m., unpaired t-test revealed p<0.0001).

References

Akiyoshi, B., K.K. Sarangapani, A.F. Powers, C.R. Nelson, S.L. Reichow, H. Arellano-Santoyo, T. Gonen, J.A. Ranish, C.L. Asbury, and S. Biggins. 2010. Tension directly stabilizes reconstituted kinetochore-microtubule attachments. *Nature*. 468:576-579.

Aravamudhan, P., R. Chen, B. Roy, J. Sim, and A.P. Joglekar. 2016. Dual mechanisms regulate the recruitment of spindle assembly checkpoint proteins to the budding yeast kinetochore. *Mol Biol Cell*. 27:3405-3417.

Aravamudhan, P., I. Felzer-Kim, K. Gurunathan, and A.P. Joglekar. 2014. Assembling the protein architecture of the budding yeast kinetochore-microtubule attachment using FRET. *Curr Biol*. 24:1437-1446.

Aravamudhan, P., A.A. Goldfarb, and A.P. Joglekar. 2015. The kinetochore encodes a mechanical switch to disrupt spindle assembly checkpoint signalling. *Nat Cell Biol*. 17:868-879.

Baum, M., and L. Clarke. 2000. Fission Yeast Homologs of Human CENP-B Have Redundant Functions Affecting Cell Growth and Chromosome Segregation. *Molecular and Cellular Biology*. 20:2852-2864.

Bouck, D.C., and K. Bloom. 2007. Pericentric chromatin is an elastic component of the mitotic spindle. *Curr Biol*. 17:741-748.

Cheeseman, I.M., S. Anderson, M. Jwa, E.M. Green, J. Kang, J.R. Yates, 3rd, C.S. Chan, D.G. Drubin, and G. Barnes. 2002. Phospho-regulation of kinetochore-microtubule attachments by the Aurora kinase Ipl1p. *Cell*. 111:163-172.

Craig, R., J.P. Cortens, and R.C. Beavis. 2004. Open source system for analyzing, validating, and storing protein identification data. *J Proteome Res*. 3:1234-1242.

Espeut, J., D.K. Cheerambathur, L. Krenning, K. Oegema, and A. Desai. 2012. Microtubule binding by KNL-1 contributes to spindle checkpoint silencing at the kinetochore. *J. Cell Biol*. 196:469-482.

Etemad, B., T.E. Kuijt, and G.J. Kops. 2015. Kinetochore-microtubule attachment is sufficient to satisfy the human spindle assembly checkpoint. *Nat Commun*. 6:8987.

Franck, A.D., A.F. Powers, D.R. Gestaut, T. Gonen, T.N. Davis, and C.L. Asbury. 2007. Tension applied through the Dam1 complex promotes microtubule elongation providing a direct mechanism for length control in mitosis. *Nat Cell Biol*. 9:832-837.

Giaever, G., A.M. Chu, L. Ni, C. Connelly, L. Riles, S. Véronneau, S. Dow, A. Lucau-Danila, K. Anderson, B. André, A.P. Arkin, A. Astromoff, M. El Bakkoury, R. Bangham, R. Benito, S. Brachat, S. Campanaro, M. Curtiss, K. Davis, A. Deutschbauer, K.-D. Entian, P. Flaherty, F. Foury, D.J. Garfinkel, M. Gerstein, D. Gotte, U. Güldener, J.H. Hegemann, S. Hempel, Z. Herman, D.F. Jaramillo, D.E. Kelly, S.L. Kelly, P. Kötter, D. LaBonte, D.C. Lamb, N. Lan, H. Liang, H. Liao, L. Liu, C. Luo, M. Lussier, R. Mao, P. Menard, S.L. Ooi, J.L. Revuelta, C.J. Roberts, M. Rose, P. Ross-Macdonald, B. Scherens, G. Schimmack, B. Shafer, D.D. Shoemaker, S. Sookhai-Mahadeo, R.K. Storms, J.N. Strathern, G. Valle, M. Voet, G. Volckaert, C.-y. Wang, T.R. Ward, J. Wilhelmy, E.A. Winzeler, Y. Yang, G. Yen, E. Youngman, K. Yu, H. Bussey, J.D. Boeke, M. Snyder, P. Philippsen, R.W. Davis, and M. Johnston. 2002. Functional profiling of the Saccharomyces cerevisiae genome. *Nature*. 418:387.

Gillett, E.S., C.W. Espelin, and P.K. Sorger. 2004. Spindle checkpoint proteins and chromosome–microtubule attachment in budding yeast. *The Journal of Cell Biology*. 164:535-546.

Haruki, H., J. Nishikawa, and U.K. Laemmli. 2008. The anchor-away technique: rapid, conditional establishment of yeast mutant phenotypes. *Mol Cell*. 31:925-932.

Hendrickx, A., M. Beullens, H. Ceulemans, T. Den Abt, A. Van Eynde, E. Nicolaescu, B. Lesage, and M. Bollen. 2009. Docking motif-guided mapping of the interactome of protein phosphatase-1. *Chem. Biol.* 16:365-371.

Hiruma, Y., C. Sacristan, S.T. Pachis, A. Adamopoulos, T. Kuijt, M. Ubbink, E. von Castelmur, A. Perrakis, and G.J. Kops. 2015. CELL DIVISION CYCLE. Competition between MPS1 and microtubules at kinetochores regulates spindle checkpoint signaling. *Science*. 348:1264-1267.

Hurley, T.D., J. Yang, L. Zhang, K.D. Goodwin, Q. Zou, M. Cortese, A.K. Dunker, and A.A. DePaoli-Roach. 2007. Structural basis for regulation of protein phosphatase 1 by inhibitor-2. *J. Biol. Chem.* 282:28874-28883.

Ji, Z., H. Gao, and H. Yu. 2015. CELL DIVISION CYCLE. Kinetochore attachment sensed by competitive Mps1 and microtubule binding to Ndc80C. *Science*. 348:1260-1264.

Joglekar, A., R. Chen, and J. Lawrimore. 2013a. A Sensitized Emission Based Calibration of FRET Efficiency for Probing the Architecture of Macromolecular Machines. *Cellular and Molecular Bioengineering*. 6:369-382.

Joglekar, A., R. Chen, and J. Lawrimore. 2013b. A Sensitized Emission Based Calibration of FRET Efficiency for Probing the Architecture of Macromolecular Machines. *Cell Mol Bioeng*. 6:369-382.

Joglekar, A.P., K. Bloom, and E.D. Salmon. 2009. In vivo protein architecture of the eukaryotic kinetochore with nanometer scale accuracy. *Curr Biol*. 19:694-699.

Joglekar, A.P., D.C. Bouck, J.N. Molk, K.S. Bloom, and E.D. Salmon. 2006. Molecular architecture of a kinetochore–microtubule attachment site. *Nature Cell Biology*. 8:581.

Joglekar, A.P., and A.A. Kukreja. 2017. How Kinetochore Architecture Shapes the Mechanisms of Its Function. *Curr Biol*. 27:R816-R824.

Jürg Bähler, Jian-Qiu Wu, Mark S. Longtine, Nirav G. Shah, Amos Mckenzie III, Alexander B. Steever, Achim Wach, Peter Philippsen, and J.R. Pringle. 1998. Heterologous modules for efficient and versatile PCR-based gene targeting in Schizosaccharomyces pombe. *YEAST*. 14:943-951.

Kawashima, S.A., Y. Yamagishi, T. Honda, K.-i. Ishiguro, and Y. Watanabe. 2010a. Phosphorylation of H2A by Bub1 Prevents Chromosomal Instability Through Localizing Shugoshin. *Science*. 327:172-177.

Kawashima, S.A., Y. Yamagishi, T. Honda, K. Ishiguro, and Y. Watanabe. 2010b. Phosphorylation of H2A by Bub1 prevents chromosomal instability through localizing shugoshin. *Science*. 327:172-177.

Lampson, M.A., K. Renduchitala, A. Khodjakov, and T.M. Kapoor. 2004. Correcting improper chromosome-spindle attachments during cell division. *Nat Cell Biol*. 6:232-237.

Liu, D., M. Vleugel, C.B. Backer, T. Hori, T. Fukagawa, I.M. Cheeseman, and M.A. Lampson. 2010. Regulated targeting of protein phosphatase 1 to the outer kinetochore by KNL1 opposes Aurora B kinase. *J. Cell Biol*. 188:809-820.

London, N., S. Ceto, J.A. Ranish, and S. Biggins. 2012. Phosphoregulation of Spc105 by Mps1 and PP1 regulates Bub1 localization to kinetochores. *Curr Biol*. 22:900-906.

Marco, E., J.F. Dorn, P.H. Hsu, K. Jaqaman, P.K. Sorger, and G. Danuser. 2013. S. cerevisiae chromosomes biorient via gradual resolution of syntely between S phase and anaphase. *Cell*. 154:1127-1139.

Meadows, John C., Lindsey A. Shepperd, V. Vanoosthuyse, Theresa C. Lancaster, Alicja M. Sochaj, Graham J. Buttrick, Kevin G. Hardwick, and Jonathan B.A. Millar. 2011. Spindle Checkpoint Silencing Requires Association of PP1 to Both Spc7 and Kinesin-8 Motors. *Developmental Cell*. 20:739-750.

Nijenhuis, W., G. Vallardi, A. Teixeira, G.J. Kops, and A.T. Saurin. 2014. Negative feedback at kinetochores underlies a responsive spindle checkpoint signal. *Nat Cell Biol*. 16:1257-1264.

Pearson, C.G., P.S. Maddox, T.R. Zarzar, E.D. Salmon, and K. Bloom. 2003. Yeast Kinetochores Do Not Stabilize Stu2p-dependent Spindle Microtubule Dynamics. *Molecular Biology of the Cell*. 14:4181-4195.

Peplowska, K., A.U. Wallek, and Z. Storchova. 2014. Sgo1 regulates both condensin and Ipl1/Aurora B to promote chromosome biorientation. *PLoS Genet*. 10:e1004411.

Pinsky, B.A., C.V. Kotwaliwale, S.Y. Tatsutani, C.A. Breed, and S. Biggins. 2006a. Glc7/protein phosphatase 1 regulatory subunits can oppose the Ipl1/aurora protein kinase by redistributing Glc7. *Mol Cell Biol*. 26:2648-2660.

Pinsky, B.A., C. Kung, K.M. Shokat, and S. Biggins. 2006b. The Ipl1-Aurora protein kinase activates the spindle checkpoint by creating unattached kinetochores. *Nat Cell Biol*. 8:78-83.

Posch, M., G.A. Khoudoli, S. Swift, E.M. King, J.G. Deluca, and J.R. Swedlow. 2010. Sds22 regulates aurora B activity and microtubule-kinetochore interactions at mitosis. *J. Cell Biol*. 191:61-74.

Primorac, I., J.R. Weir, E. Chiroli, F. Gross, I. Hoffmann, S. van Gerwen, A. Ciliberto, and A. Musacchio. 2013. Bub3 reads phosphorylated MELT repeats to promote spindle assembly checkpoint signaling. *Elife*. 2:e01030.

Rosenberg, J.S., F.R. Cross, and H. Funabiki. 2011. KNL1/Spc105 recruits PP1 to silence the spindle assembly checkpoint. *Curr Biol*. 21:942-947.

Salic, A., J.C. Waters, and T.J. Mitchison. 2004. Vertebrate shugoshin links sister centromere cohesion and kinetochore microtubule stability in mitosis. *Cell*. 118:567-578.

Scott, R.J., C.P. Lusk, D.J. Dilworth, J.D. Aitchison, and R.W. Wozniak. 2005. Interactions between Mad1p and the nuclear transport machinery in the yeast Saccharomyces cerevisiae. *Mol Biol Cell*. 16:4362-4374.

Suijkerbuijk, Saskia J.E., M. Vleugel, A. Teixeira, and Geert J.P.L. Kops. 2012. Integration of Kinase and Phosphatase Activities by BUBR1 Ensures Formation of Stable Kinetochore-Microtubule Attachments. *Developmental Cell*. 23:745-755.

Suzuki, A., A. Gupta, S.K. Long, R. Evans, B.L. Badger, E.D. Salmon, S. Biggins, and K. Bloom. 2018. A Kinesin-5, Cin8, Recruits Protein Phosphatase 1 to Kinetochores and Regulates Chromosome Segregation. *Curr Biol*. 28:2697-2704 e2693.

Tanaka, T.U., N. Rachidi, C. Janke, G. Pereira, M. Galova, E. Schiebel, M.J. Stark, and K. Nasmyth. 2002. Evidence that the Ipl1-Sli15 (Aurora kinase-INCENP) complex promotes chromosome bi-orientation by altering kinetochore-spindle pole connections. *Cell*. 108:317-329.

Tatchell, K., V. Makrantoni, M.J. Stark, and L.C. Robinson. 2011. Temperature-sensitive ipl1-2/Aurora B mutation is suppressed by mutations in TOR complex 1 via the Glc7/PP1 phosphatase. *Proc Natl Acad Sci USA*. 108:3994-3999.

Tauchman, E.C., F.J. Boehm, and J.G. DeLuca. 2015. Stable kinetochore-microtubule attachment is sufficient to silence the spindle assembly checkpoint in human cells. *Nat Commun*. 6:10036.

Verma, V., L. Mallik, R.F. Hariadi, S. Sivaramakrishnan, G. Skiniotis, and A.P. Joglekar. 2015. Using Protein Dimers to Maximize the Protein Hybridization Efficiency with Multisite DNA Origami Scaffolds. *PLoS One*. 10:e0137125.

Verzijlbergen, K.F., O.O. Nerusheva, D. Kelly, A. Kerr, D. Clift, F. de Lima Alves, J. Rappsilber, and A.L. Marston. 2014. Shugoshin biases chromosomes for biorientation through condensin recruitment to the pericentromere. *Elife*. 3:e01374.

Welburn, J.P.I., M. Vleugel, D. Liu, J.R. Yates Iii, M.A. Lampson, T. Fukagawa, and I.M. Cheeseman. 2010. Aurora B Phosphorylates Spatially Distinct Targets to Differentially Regulate the Kinetochore-Microtubule Interface. *Molecular Cell*. 38:383-392.

Xu, Z., B. Cetin, M. Anger, U.S. Cho, W. Helmhart, K. Nasmyth, and W. Xu. 2009. Structure and function of the PP2A-shugoshin interaction. *Mol Cell*. 35:426-441.